GREEN SYNTHESIS AND CHARACTERIZATION OF SILVER NANOPARTICLES FOR THEIR ANTIOXIDANT AND PHOTOCATALYTIC STUDIES

Chethan K S
Department of Organic Chemistry, V. V puram College of Science, Bangalore, Karnataka.
Email: chethu0533@gmail.com

Abstract
In this study, silver nanoparticles (Ag NPs) were successfully synthesized from neem leaves using the solution combustion method (SCM). The synthesized Ag was systematically characterized using XRD, SEM, UV-Vis, and FTIR spectroscopy. XRD analysis confirmed the crystalline nature of the nanoparticles, with an average particle size of approximately 15 nm. SEM images revealed a spherical morphology with uniform distribution. UV-Vis showed a characteristic absorption peak around 450 nm, corresponding to an energy band gap of 2.31 eV. FTIR identified the stretching and bending vibrations of metal-oxide bonds, confirming the formation of Ag. The antioxidant potential of Ag was evaluated using DPPH, ABTS, FRAP, and FICA assays, with ascorbic acid as the standard. The nanoparticles exhibited significant antioxidant activity, achieving 92%, 94%, 93%, and 95% inhibition at concentrations of 500 µg/mL. Furthermore, the photocatalytic efficiency of Ag was assessed against various azo dyes, including Malachite Green (MG), Orange G (OG), Rose Bengal (RB), and Methyl Violet (MV). The degradation efficiencies were 95.15%, 97.02%, 94.41%, and 96.87%, respectively, at an initial dye concentration of 5 ppm within 10 minutes. The reaction kinetics followed a first-order rate model, with additional investigations into half-life ($t_{1/2}$), pH influence, scavenger effects, and catalyst recyclability. Overall, the synthesized Ag demonstrated excellent antioxidant and photocatalytic performance, highlighting their potential for environmental remediation and biomedical applications.

Keywords: *Silver, SCM, Characterization, Antioxidant, Photocatalysis.*

1. INTRODUCTION

In recent years, various chemical and electrochemical methods have been actively explored for the synthesis of silver nanoparticles (Ag NPs), aiming to improve their stability, size control, and functional properties [1]. The use of hazardous chemicals or the generation of unwanted byproducts that require energy-intensive handling pose significant challenges for many of these techniques, particularly during the purification phase [2]. Nanoparticles can be synthesized using a variety of materials, including metal oxides, metals, silicates, and non-oxide ceramics. Among the different synthesis techniques, chemical reduction and electrochemical methods are currently the most widely employed due to their efficiency and scalability [3]. One of the common challenges researchers face is controlling the size and shape of nanoparticles while achieving monodispersity, which is crucial for their stability and functional performance [4]. To address these challenges, environmentally friendly techniques have been developed by incorporating biological principles into the synthesis process, such as utilizing microorganisms or plant extracts [5]. These green approaches offer a sustainable alternative by reducing the reliance on hazardous chemicals while enhancing biocompatibility [5]. In addition to hard template methods, nanomaterials such as Au, Ag, Pt, and Pd can also be synthesized using biological approaches, including fungi [7], bacteria [8], and plant extracts [9-10]. These green synthesis methods offer sustainable and eco-friendly alternatives for nanoparticle production [6]. One key advantage of utilizing plant resources for nanoparticle synthesis is that it eliminates the need for complex procedures such as chemical purification and the maintenance of microbial cell cultures, making the process more straightforward and cost-effective [11]. Most environmentally friendly methods reported in the literature face challenges related to particle aggregation, stability, and controlled crystal growth [12]. However, silver compounds have been extensively studied since ancient times for their strong antibacterial and inhibitory properties, making them valuable in the prevention and treatment of infections [13]. Research indicates that biosynthesized silver nanoparticles exhibit a range of beneficial properties, including antiviral, antibacterial, anti-inflammatory, anti-angiogenic, antioxidant, and anti-platelet effects [14]. Notably, Fatimah successfully harnessed the natural compounds present in P. speciosa Hassk pods and combined them with microwave irradiation to synthesize silver nanoparticles specifically for antibacterial applications [15]. In 2018, Yusof et al. used P. speciosa leaf extract to synthesize and analyze silver nanoparticles (Ag NPs) [16]. The researchers prepared the Ag NPs by allowing the leaf extract to react at room temperature overnight, enabling a simple and eco-friendly approach for nanoparticle production and characterization [16]. Both studies demonstrated that *P. speciosa* can function as a capping and reducing agent in the synthesis of silver nanoparticles (Ag NPs). Similarly, neem leaves, with their rich phytochemical composition, offer several advantages for Ag NP synthesis, enhancing stability and providing additional bioactive properties [16].

Neem is widely recognized for its abundance of bioactive compounds, such as terpenoids, alkaloids, and flavonoids, which serve as capping and reducing agents in nanoparticle synthesis, enhancing their stability and functionality [17]. These bioactive compounds not only facilitate the reduction of silver ions into nanoparticles but also impart additional properties to the synthesized nanoparticles, including antioxidant, antibacterial, antifungal, and antiviral activities [18]. This dual functionality enhances the effectiveness of neem leaf-mediated silver nanoparticles across various applications, ranging from biomedical uses in combating infections and oxidative stress to environmental remediation through photocatalysis [19]. Consequently, neem leaves offer not only an eco-friendly and sustainable approach to nanoparticle synthesis but also impart diverse biological properties to the nanoparticles, making them highly suitable for various scientific and technological applications [20].

The unique physical and chemical properties of metallic nanoparticles make them highly versatile, enabling researchers to explore their applications across various fields, including electronics, biosensors, food preservation, textiles, healthcare, environmental remediation, and agriculture [21-22]. Due to their excellent catalytic activity, metallic nanoparticles have recently garnered significant attention for their application in the degradation of hazardous dyes, offering an efficient and sustainable solution for wastewater treatment [22]. Nanoparticles required for the catalytic degradation of textile dyes can be synthesized using various physical, chemical, and biological methods, each offering distinct advantages in terms of efficiency, scalability, and environmental sustainability [23-24]. Biological approaches utilize plants, bacteria, fungi, and algae as raw materials for silver nanoparticle synthesis, offering a sustainable alternative, whereas physical methods often demand high energy inputs to achieve nanoparticle formation [25]. However, chemical synthesis of silver nanoparticles is more versatile, enabling precise control over their stability, size, and shape, making it a widely preferred method for nanoparticle production [25]. Nanoparticles have been extensively studied for their catalytic activity in the degradation of various toxic dyes, including Auramine O, Thymol Blue, Rhodamine B, Congo Red, Phloxine B, Methyl Orange, and others [26-28]. Several dyes have been reported to degrade by up to 90–100% upon exposure to silver nanoparticles. Moreover, the nanoparticle-based dye degradation process is not only rapid but also eliminates the need for hazardous chemicals commonly associated with traditional chemical and biological wastewater treatment methods [29]. Recently, green-synthesized AgNPs have demonstrated effective dye degradation capabilities for Methyl Orange, Methyl Red, and Congo Red individually [30]. In a related study, AgNPs synthesized using *Sophora mollis* leaf extract achieved 88% degradation of Methylene Blue within 160 minutes, highlighting their potential for efficient and eco-friendly wastewater treatment [31]. A study also highlighted the promising potential of AgNPs for degrading Methylene Blue [32]. However, a review of the literature reveals that most studies focus solely on the catalytic activity of silver nanoparticles for individual dyes, whereas real wastewater typically contains a complex mixture of multiple dyes. Although only a limited number of studies have explored the catalytic activity of silver nanoparticles for multiple dyes commonly found in wastewater [33], investigating their degradation potential in complex dye mixtures is essential for developing more effective and practical wastewater treatment solutions [34-35].

This study explores the green synthesis of silver nanoparticles (Ag NPs) using neem leaf extract via the solution combustion method (SCM). Characterization via XRD, SEM, UV-Vis, and FTIR confirmed their crystalline nature (~15 nm size), spherical morphology, and strong optical absorption at ~450 nm (2.31 eV band gap). Ag NPs exhibited excellent antioxidant activity in DPPH, ABTS, FRAP, and FICA assays and achieved >94% photocatalytic degradation of azo dyes within 10 minutes. Reaction kinetics, pH influence, scavenger effects, and recyclability were also examined. These highlight Ag NPs' potential for environmental remediation and biomedical applications.

2. MATERIALS AND METHODS

2.1. Chemicals utilized

The chemicals in the experiment were of analytical grade and used without any modifications. There are only two chemicals, including silver nitrate ($AgNO_3$) and deionized water.

2.2. Preparation of Neem powder

The neem leaves were freshly harvested and washed with double-distilled water. They were dried in the sun for one week before being ground into a powder with a mortar. This powder was then stored in an airtight container for the synthesis of the nanomaterial.

2.3. Green synthesis of Ag nanoparticle

In the synthesis of Ag nanoparticles via the solution combustion method, neem leaves were used as the fuel source. A mixture consisting of 0.5 g silver nitrate and 0.25 g neem leaf powder in a 2:1 ratio was prepared. This mixture was dissolved in 15 mL of water, transferred to a silica crucible, and heated at 800 °C for 60 minutes in a muffle furnace [36].

3. RESULTS AND DISCUSSION

3.1. XRD

The XRD pattern of the silver nanoparticle is shown in Fig. 1. The 2θ values of 27.81°, 32.16°, 38.12°, 44.3°, 46.21°, 54.83°, 57.39°, 64.42°, and 77.45° correspond to Bragg reflection peaks. These peaks correspond to the (210), (122), (111), (200), (231), (142), (241), (220), and (311) planes of silver, as indicated by the face-centered cubic structure (FCC) (JCPDS file No. 04-0783) [37-38]. The XRD measurements conclusively show that the extract results in the formation of solid Ag nanoparticles. The particle size of the Ag nanoparticle was evaluated using Debye-Scherer's Eq (1) [39],

$$\mathbf{D = \frac{0.9\lambda}{\beta cos\theta} \dots\dots (1)}$$

Here, D represents the crystalline size, λ is the X-ray wavelength, β denotes the FWHM of the diffraction peak, and θ is Bragg's angle. The nanoparticle size for the (111) plane was 15 nm [40].

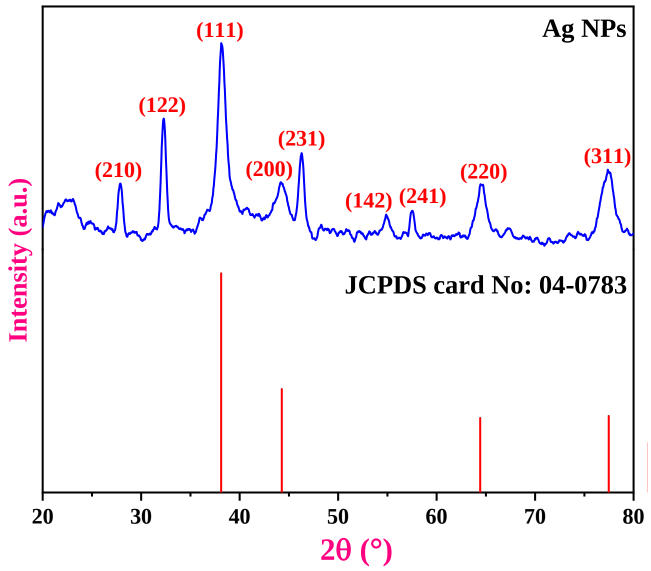

Fig. 1. XRD of Ag NPs.

3.2. FTIR

The FTIR spectrum of silver nanoparticles is shown in Fig. 2. The metal nanoparticles undergo stabilization, capping, and reduction due to the plant extracts. The transmission peaks at 558, 1013, 1342, 1627, 2346, and 3248 cm^{-1} were measured [41]. The peak around 1376 cm^{-1} is attributed to C-N and O-H bending, while the 1042 cm^{-1} band indicates the -C-O stretching vibration of -OH groups. The peak indicates the C=C group vibration modes at 1605 cm^{-1}, whereas the larger peak at 3253.76 cm^{-1} corresponds to the O-H and C=O bands, which are characteristic of aliphatic carboxylic acid functional groups [42]. The stretching mode at 1605 cm^{-1} represents the N-H bond, which is characteristic of the amine band. According to FTIR data, silver can attach to biological molecules containing protein carboxylate groups [43]. The reduction process leads to a decrease in intensity at 3433 cm^{-1}, indicating the participation of a phenolic functional group from neem leaves. These peaks were mostly attributed to the abundance of flavonoids and terpenoids present in the plant extract [44]. The synthesized silver nanoparticles are bound to alcoholic groups, proteins, carboxylate groups, and stretching vibration modes [45].

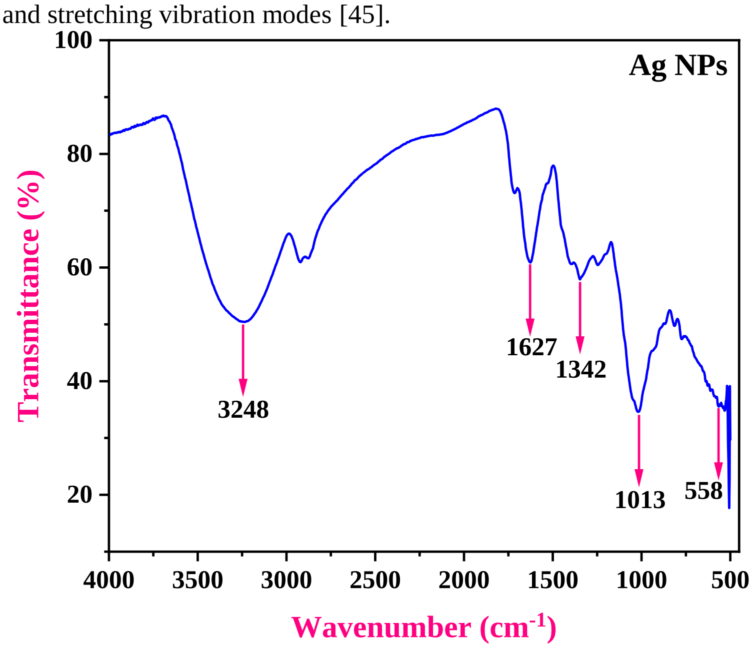

Fig. 2. FTIR of Ag NPs.

3.3. UV-Vis and Tauc's plot

The UV-Vis and Tauc's plot spectrum of silver nanoparticles was displayed in Fig. 3. Fig. 3(a) shows that the generation of Ag NPs is confirmed by the SPR band centered at 442 nm, as observed in the UV-Vis. The observed peak is due to Surface Plasmon Resonance, a quantum-mechanical phenomenon that depends on nanoparticle size [46]. This phenomenon becomes significant when the size of the particle is smaller than or equal to the De-Broglie wavelength of the valence electrons. A band at 264 nm, corresponding to the n-$\pi*$ transition, appears in the UV-Vis spectra of the leaf extract [47]. In Fig. 3(b), the graph illustrates $(h\nu)^2$ as a function of photon energy (hν) for Ag NPs. The energy band gap (Eg) was calculated using Eq. (2) from previously published sources [48].

$$\alpha = \frac{A(h\nu - E_g)^{n/2}}{h\nu}$$

Here, α represents the absorption coefficient, hν stands for photon energy, A is a constant, and Eg denotes the band gap energy. The band gap of Ag NPs, as seen in Fig. 3(b), is 2.31 eV [49-50].

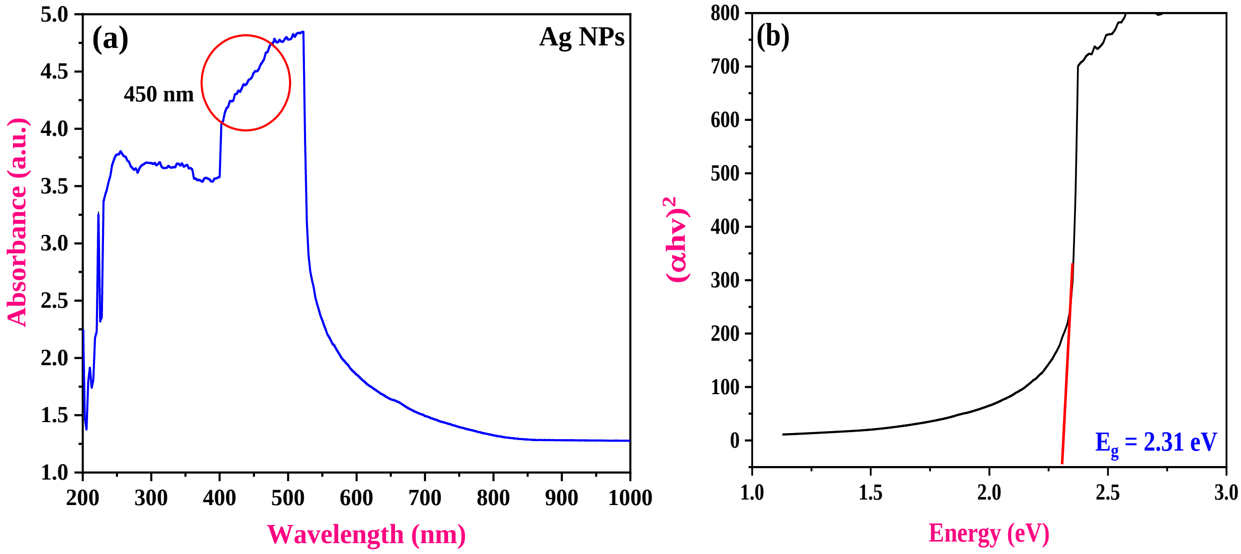

Fig. 3. (a) UV-Vis and (b) Tauc's plot of Ag NPs.

3.4. FESEM

The FESEM analysis of silver nanoparticles is shown in Fig. 4. The image depicts particles with a small, spherical-like form, exhibiting high uniformity in size and consistent distribution over the area, with surrounding vacuum space shown in Fig. 4(a) [51]. At high magnification, the image reveals particle breakdown, high agglomeration, uniform spacing between particles, and uniform particle size. At high magnification, the image reveals particle breakdown with high agglomeration, uniform spacing between particles, and uniform particle size, as shown in Fig. 4(b) [52].

Fig. 4. FESEM image of Ag NPs (a) 20 µm and (b) 2 µm.

4. ANTIOXIDANT STUDIES

4.1. DPPH and ABTS assay

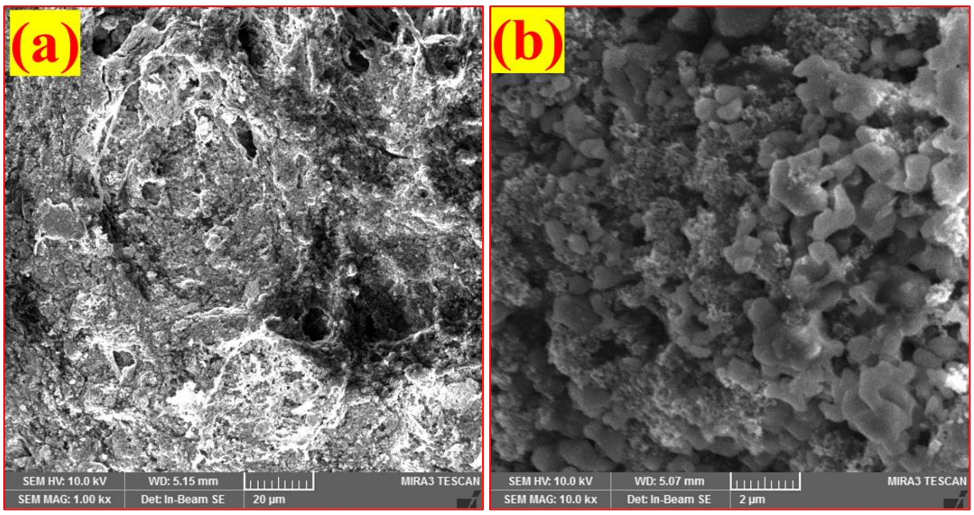

Antioxidants are molecules that prevent damage caused by free radicals, which are produced by numerous biological systems and can affect cellular and biological processes [53]. The DPPH and ABTS techniques are commonly used to assess a material's antioxidant activity, serving as effective analytical methods for measuring free radical scavenging ability [54]. The ABTS test generates a blue-green ABTS$\bullet^+$ radical, which is used to quantify antioxidant activity. This assay measures the ability of antioxidants to neutralize the ABTS$\bullet^+$ radical, and is effective for assessing both hydrophilic and lipophilic antioxidant systems [55]. Both the DPPH and ABTS assays depend on a proton to stabilize free radicals, using their redox-active properties to assess antioxidant activity. The DPPH and ABTS radicals react in water primarily through the SPLET process, which stands for Single Electron Transfer-Proton Transfer [56]. This process involves transferring a single electron and a proton to neutralize the radicals, thereby facilitating the measurement of antioxidant activity. In the SPLET mechanism, antioxidants and radicals act together to partially ionize phenols and alcohols in water and alcoholic solutions [57]. This process involves a single-electron transfer followed by a proton transfer, thereby facilitating the neutralization of free radicals and the measurement of antioxidant activity.

The reactivity levels of antioxidants can differ among various assays because physical factors like pH, temperature, and solvent conditions can impact the rates at which antioxidants react in each assay [58]. In Fig. 5(a-b), the DPPH and ABTS radical scavenging abilities of the synthesized nanomaterials are compared to those of ascorbic acid, a well-known conventional antioxidant, to evaluate their effectiveness in antioxidant activity. The results indicate that green-synthesized Ag NPs exhibit strong antioxidant properties, with DPPH radical-scavenging activity of 92% and ABTS radical-scavenging activity of 94% at a concentration of 500 µg/mL, demonstrating their effectiveness in neutralizing free radicals. Initially, DPPH exhibited a high absorbance, but this decreased as the dark violet color faded, reflecting the gradual reduction of DPPH radicals due to antioxidant activity [59]. The Ag NPs produced through biogenic methods demonstrate significant antibacterial and antioxidant activities, highlighting their potential for application in the pharmaceutical industry in the development of new drugs aimed at addressing oxidative stress and bacterial infections [60].

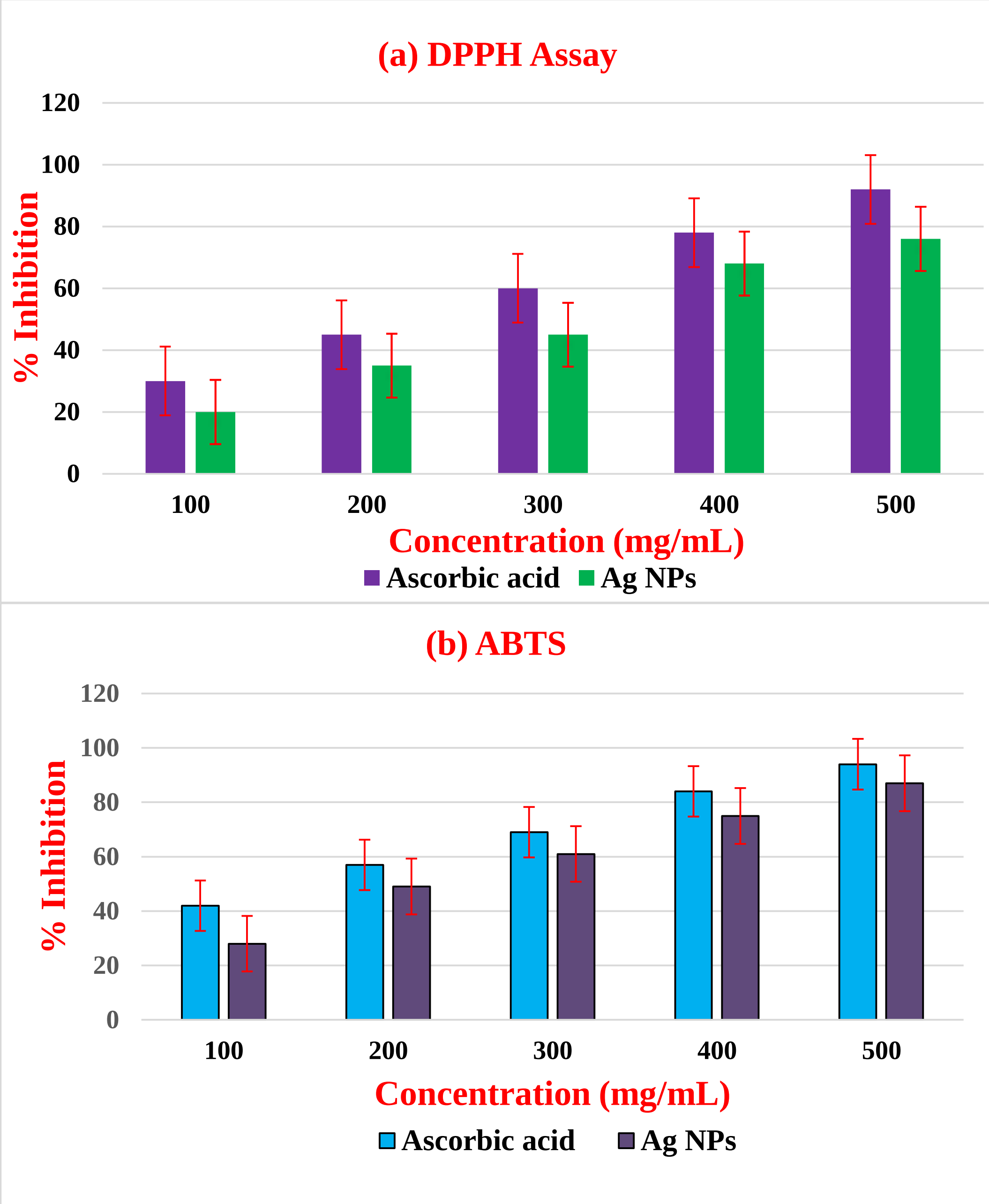

Fig. 5. Antioxidant studies of Ag NPs (a) DPPH, and (b) ABTS.

4.2. FRAP and FICA assay

The FRAP test measures the reduction of ferric to ferrous ions by nanoparticles, which serves as an indicator of their antioxidant capacity. This method evaluates how effectively the nanoparticles can neutralize free radicals. Researchers frequently use the FRAP test to measure the antioxidant activity of foods and nutritional supplements containing polyphenols [61]. This test is preferred because it relies on the electron-transfer mechanism to assess antioxidant capacity, unlike methods based on hydrogen atom transfer. The FRAP assay involves the reduction of ferric ions to ferrous ions, resulting in a blue solution. The intensity of this blue color, measured at 594 nm, correlates with the sample's activity [62]. In the FRAP test, the potential of the nanomaterial is assessed by measuring the intensity of the blue color that results from the reduction of ferric to ferrous ions. Greater blueness signifies higher antioxidant activity. Researchers favor the FRAP test for its versatility, high-throughput capabilities, and sensitivity in detecting antioxidant activity at concentrations as low as 0.3 mM Fe^{2+}, making it a reliable method for antioxidant assessment [63]. The FRAP test is an essential tool for studying antioxidants and ROS-induced stress, providing a reliable and straightforward method for quantifying antioxidant levels across a wide range of nanomaterials. This test is valuable for both research and practical applications in oxidative stress studies. The FRAP test measures antioxidant activity by reducing the colorless $[Fe(III)(TPTZ)_2]^{3+}$ complex to the intensely blue $[Fe(II)(TPTZ)_2]^{2+}$ complex in an acidic environment [64]. This color change is used to determine the sample's antioxidant capacity. A deep blue hue emerges after the reduction process, and its intensity can be quantitatively measured at 595 nm using spectrophotometry. This measurement is used to assess the antioxidant capacity of the sample. According to the results of this investigation, the ferric-reducing antioxidant power showed increased activity with higher sample concentrations, indicating a direct relationship between concentration and antioxidant effectiveness. The absorbance of the ascorbic acid (0.78–1.32) and Ag NPs (0.52–0.63) samples showed a proportionate rise in FRAP activity when the solution concentration rose in both samples from 100 to 500 µg/mL, as shown in Fig. 6(a) [65].

Nanoparticles in solution interact with $Fe2^{+}$ ions, demonstrating their ability to chelate ferrous ions and indicating their potential for metal ion sequestration. The ability of nanoparticles to chelate metal ions makes this interaction crucial for a variety of applications, including biological uses, water filtration, and protection against metal poisoning. The chelating assay is a method used to evaluate a material's binding affinity for ferrous ions [66]. This assay assesses the ability of compounds to inhibit the formation of potentially dangerous hydroxyl radicals, making it crucial for evaluating antioxidant properties and understanding their potential to protect against oxidative damage. The assay measures the absorbance of complexes generated by using a chelating agent, such as ferrozine. EDTA is frequently utilized as a positive control in FICA tests due to its well-documented ability to chelate ferrous ions in a dosage-dependent manner, providing a reliable benchmark for assessing chelating efficiency [67]. Fig. 6(b) illustrates that bio-genic Ag NPs effectively chelate metal ions, particularly converting ferric to ferrous ions, showcasing their potential for diverse applications. The solution, EDTA, exhibited the highest concentration of Fe^{2+} ions and the highest chelating activity. In contrast, Ag NPs showed chelating activity of 80% at a concentration of 100 µg/mL, highlighting the substantial yet comparatively lower efficiency of the nanoparticles [68].

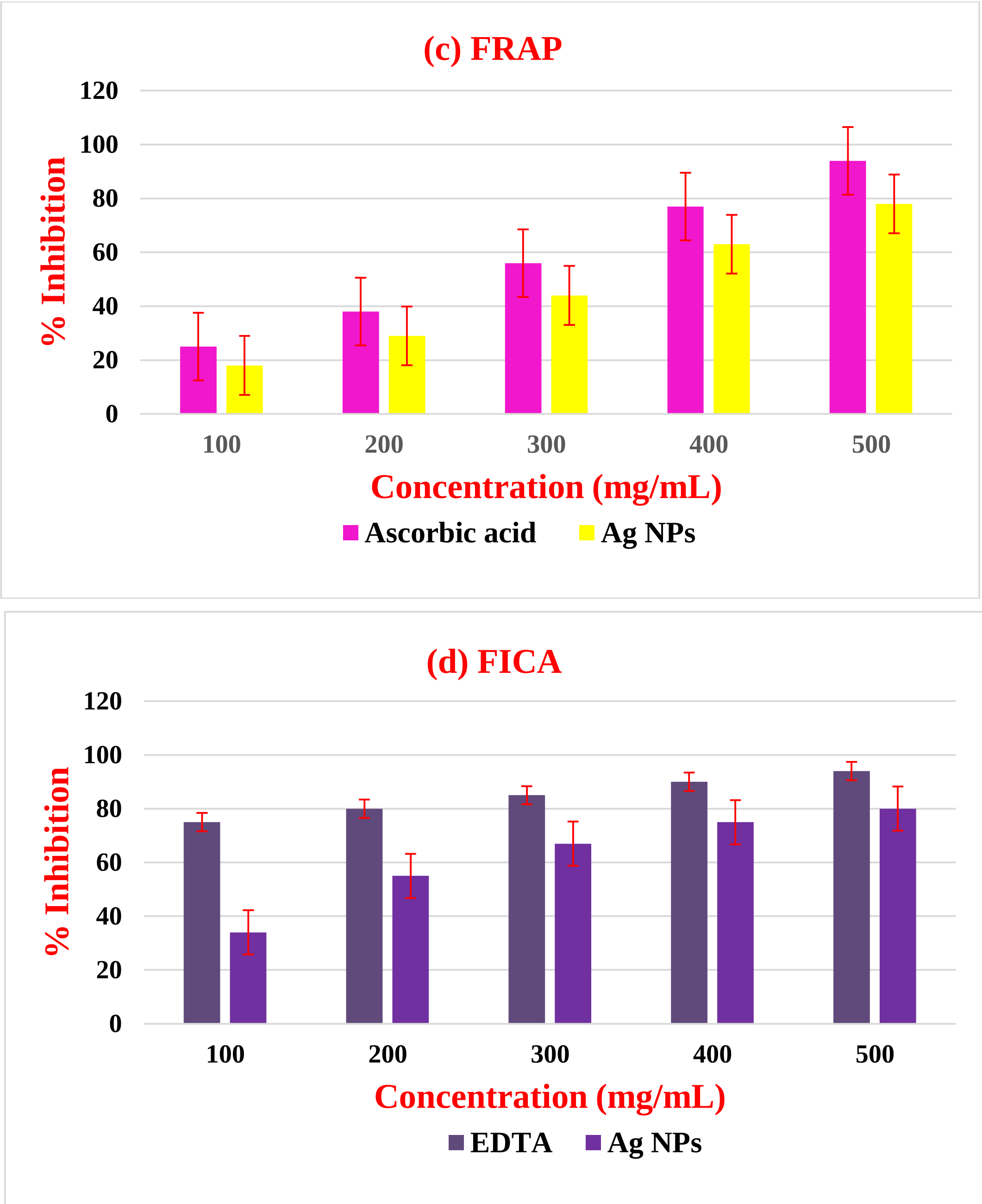

Fig. 6. Antioxidant studies of Ag NPs (a) FRAP, and (b) FICA.

5. PHOTOCATALYSIS ACTIVITY

The synthesized Ag compound was used to photodegrade MG, OG, RB, and MV dyes under UV light. The experiment was conducted at room temperature using a 150 W Philips UV lamp for the photocatalytic process, with 20 mg of catalyst dispersed in 100 mL of dye solution to evaluate its degradation efficiency. The dye concentration was monitored over time by measuring the maximum wavelength at consistent 10-minute intervals, revealing a significant decrease as the reaction progressed. The percentage of dye degradation was then calculated using Eq. (2) [69-70],

$$\%\mathbf{D} = \mathbf{C_a} - \frac{\mathbf{C_b}}{\mathbf{C_a}} * \mathbf{100} \ldots .(\mathbf{2})$$

Here, C_a and C_b are the initials. and final dye conc.

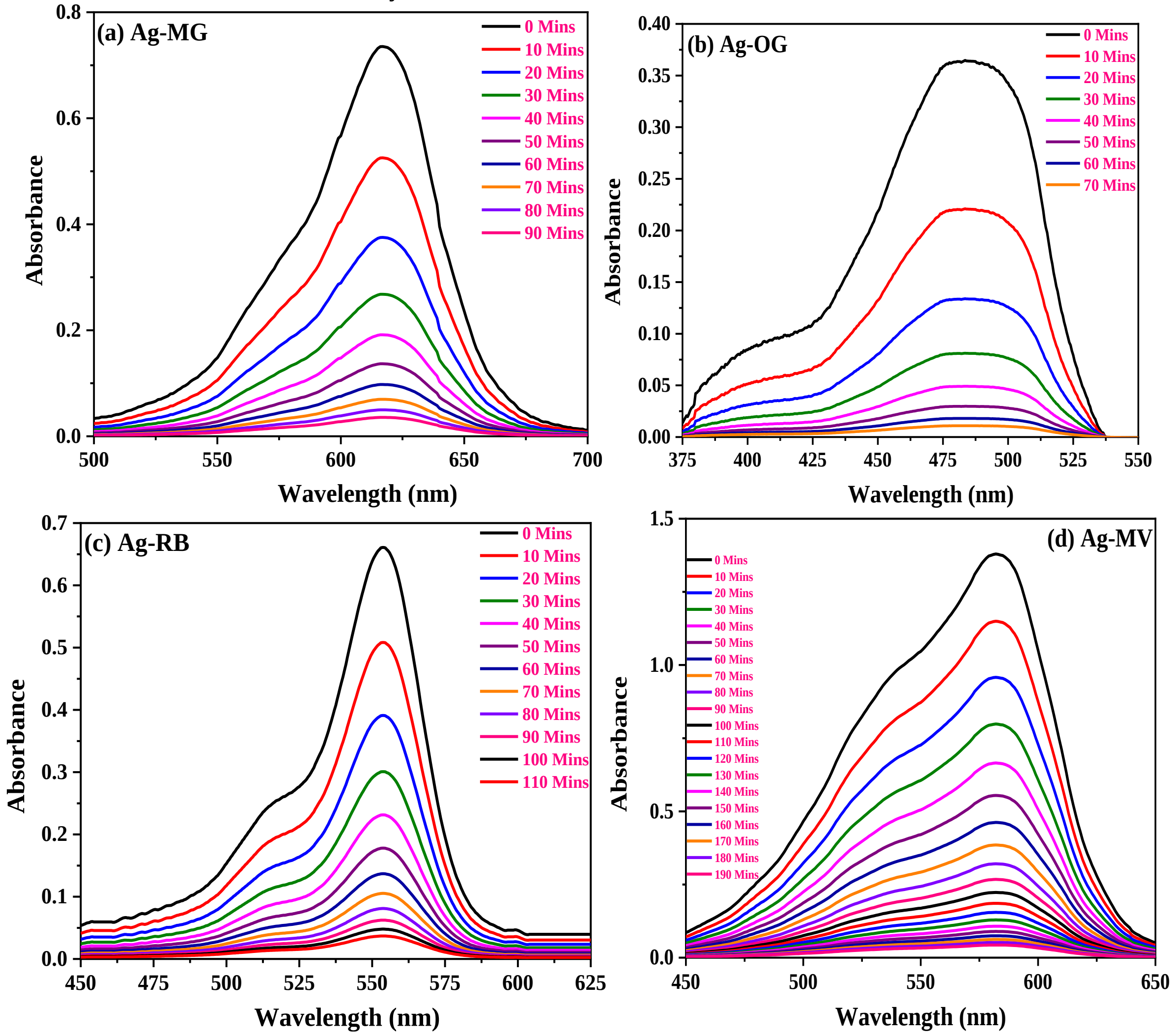

Fig. 7. UV spectrum of (a) MG, (b) OG, (c) RB, and (d) MV dye using the prepared Ag.

The degradation of MG, OG, RB, and MV dyes using Ag nanoparticles under UV light is illustrated in Fig. 7. The catalytic experiments were conducted in a standard 100 mL beaker with an approximate surface area of 50 mm, utilizing a 150 W Philips UV lamp as the irradiation source [71]. The UV-Vis spectrometer used in the study operated without any filters, with an emission wavelength range of approximately 400–800 nm in the UV spectrum and a scanning range of 190–800 nm. A 15-cm light source was employed to facilitate the reaction at room temperature (RT), and double-distilled (DD) water was used throughout the experiment. Following the standard procedure, a 5 ppm dye solution was prepared and mixed with 100 mL of 20 mg catalyst, and the mixture was continuously stirred at 500 rpm using a magnetic stirrer to ensure uniform dispersion [72-73].

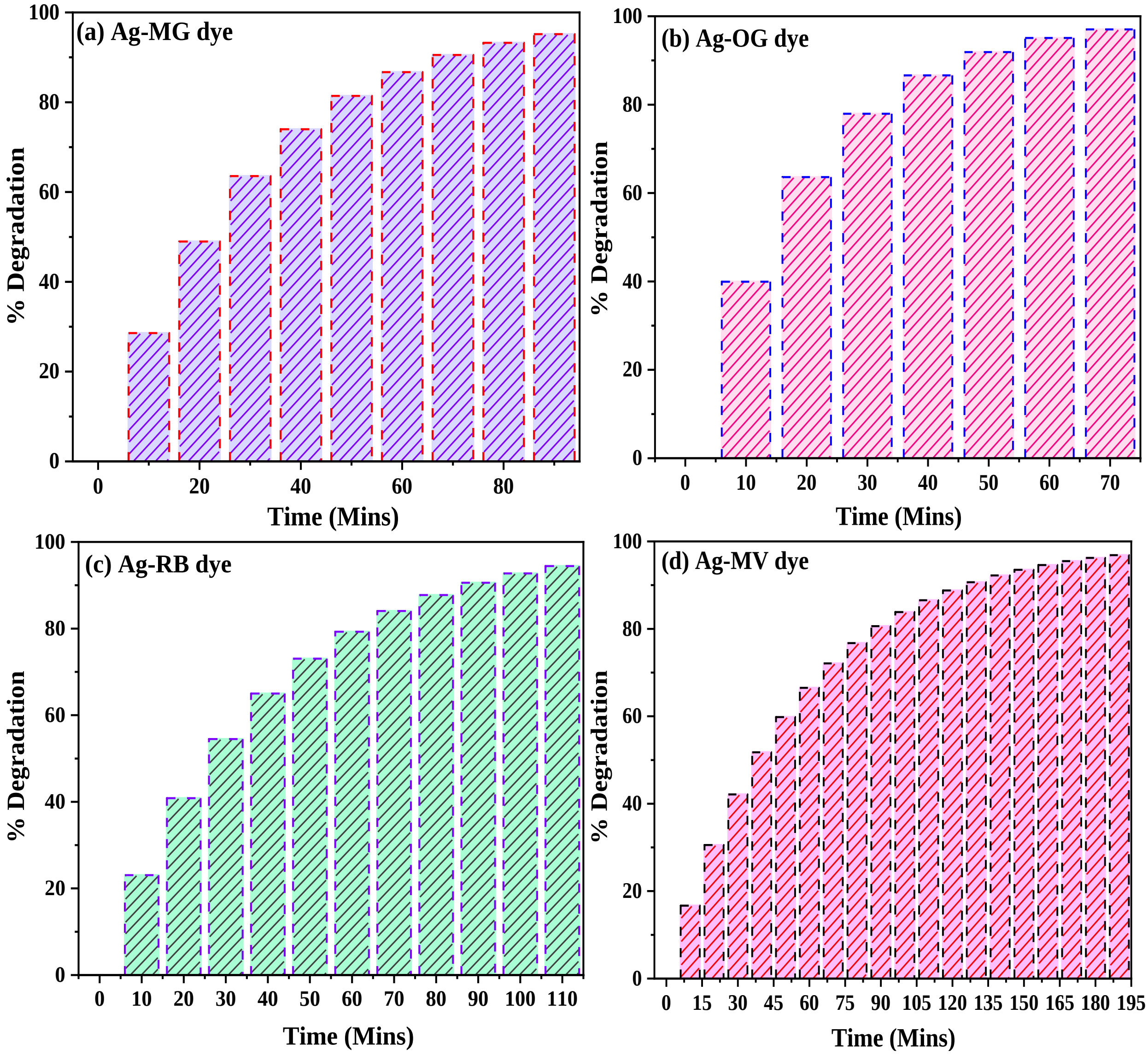

Fig. 8. % Degradation of (a) MG, (b) OG, (c) RB, and (d) MV dye using the prepared Ag.

For all measurements, the same catalyst, time intervals, dye concentration, and dye volume were used to ensure consistent conditions during the analysis of the degradation of MG, OG, RB, and MV dyes [74]. During the Ag nanoparticle photocatalytic experiments, approximately 3 mL of dye solution was collected every 10 minutes to monitor dye decolorization under the UV light source [75]. Non-environmentally friendly dyes such as MG, OG, RB, and MV can contribute to water pollution, each exhibiting a distinct maximum wavelength, as shown in Fig. 7(a-d). Initial experiments conducted in the dark during the early stages of the photocatalytic study showed no significant dye degradation, confirming that light is a crucial factor for effective photocatalysis [76]. The degradation of MG, OG, RB, and MV dyes using the synthesized Ag nanoparticles is illustrated in Fig. 8(a-d), with corresponding degradation efficiencies of approximately 95.15%, 97.02%, 94.41%, and 96.87%, respectively. Photocatalytic investigations were conducted under UV light, with measurements taken at 10-minute intervals to monitor the degradation pathway of each dye [77]. In an ideal scenario, when photons with energy greater than or equal to the band gap strike the nanomaterial, they induce charge separation, initiating the photocatalytic process. For all measurements, the same catalyst, time intervals, dye concentration, and dye volume were maintained, and the experiment was conducted in a dark room using a consistent setup [78]. The kinetic study plot illustrates the progressive degradation over time and confirms that the degradation process follows first-order kinetics, as analyzed using Eq. (3) displayed in Fig. 9(a-b) [79-80],

$$\mathbf{Kt = -\ln\left(\frac{C}{C_0}\right) \ldots\ldots (3)}$$

Here, K is the rate constant, t is the time (min) in the UV studies.

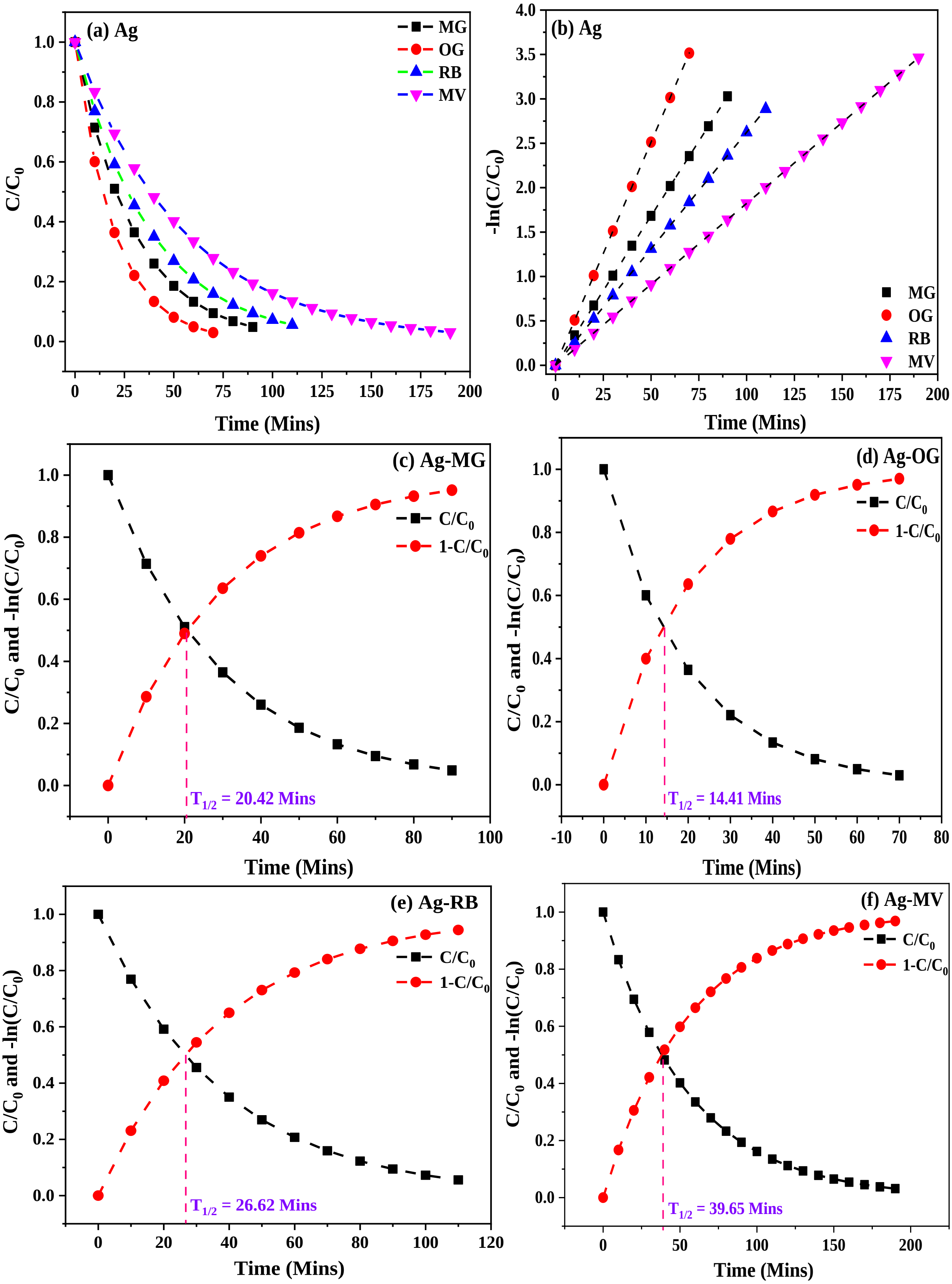

Fig. 9(a, b) Kinetic plot of dye degradation, (c-f) half-life period of dye using Ag nanoparticle.

Fig. 9(c-f) illustrates the half-life ($T_{1/2}$) of the dyes, representing the time required for 50% degradation. Using the synthesized silver nanoparticles, the half-life values were approximately 20.42 minutes for MG, 14.41 minutes for OG, 26.62 minutes for RB, and 39.65 minutes for MV dye, highlighting the varying degradation efficiencies for different dye molecules [81]. The half-life data confirm the high efficiency of Ag nanoparticles in rapidly degrading 50% of the dyes within a relatively short duration, showcasing their excellent photocatalytic performance. Additionally, the rate constant (k) values from the kinetic plot further validate the strong catalytic activity of Ag nanoparticles. A comparative analysis of silver nanoparticles, along with findings from previous studies, is presented in Table 1, providing insights into their effectiveness relative to other reported photocatalysts [82].

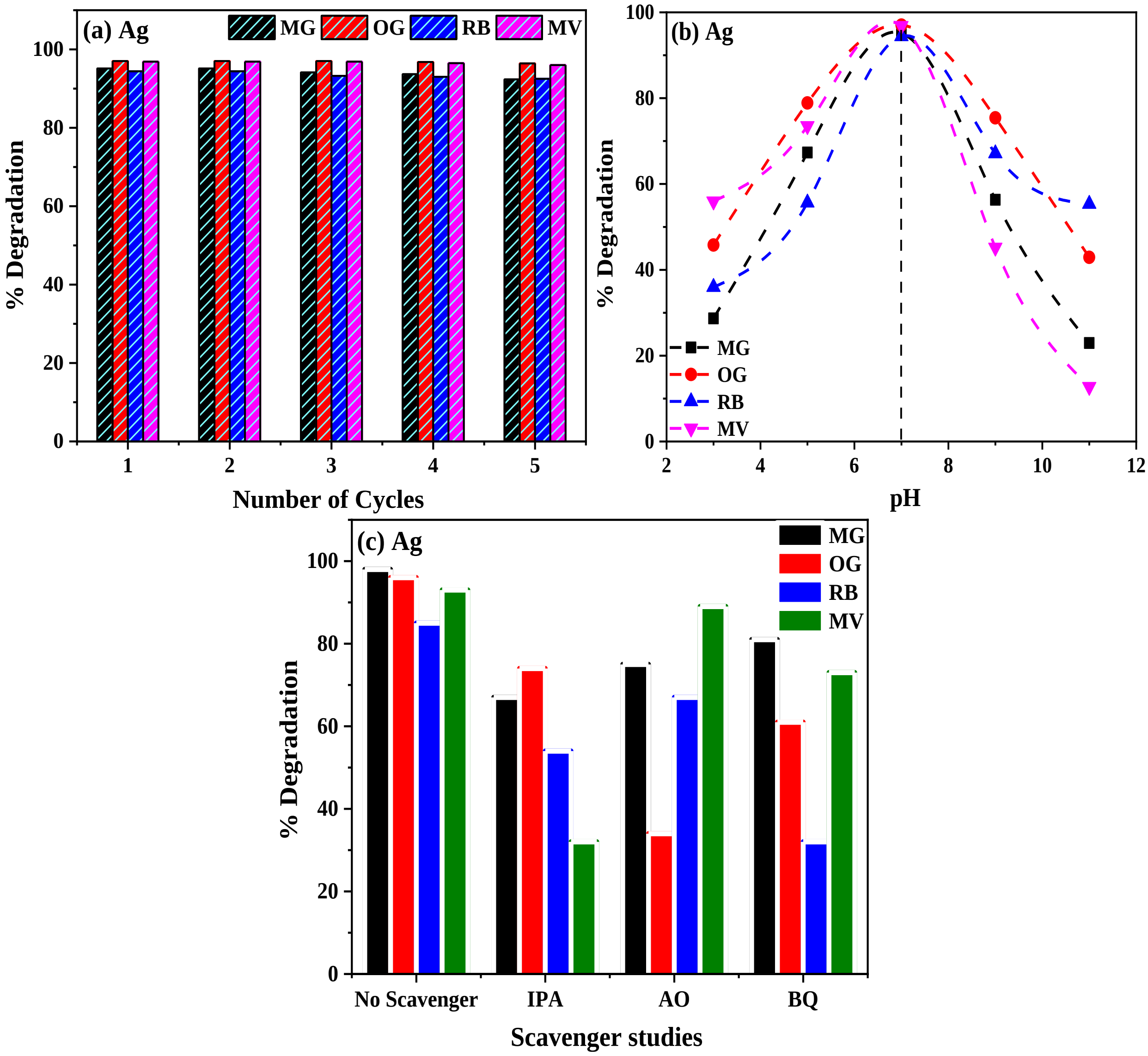

Fig. 10(a) Recyclability of the catalyst, (b) pH studies, (c) Scavenger studies.

The excellent performance of the photocatalytic degradation experiments highlights the effectiveness of Ag nanoparticles in dye decolorization. The catalyst used in this study efficiently facilitated the breakdown of azo dyes in solution, making a significant contribution to the field of photocatalytic research [83]. This process is further enhanced by the generation of reactive oxygen species, which occurs when surface oxygen interacts with conduction-band electrons, thereby playing a crucial role in the degradation mechanism. Preventing the recombination of electrons and holes is essential for achieving high photocatalytic efficiency [84]. Additionally, an increased presence of hydroxyl ions on the catalyst's surface indicates enhanced photocatalytic activity. The results of the photodegradation experiment evaluating catalyst reusability are presented in Fig. 10(a). After each cycle, the catalyst was successfully recovered using Whatman filter paper, enabling its reuse for up to five consecutive cycles without significant loss of efficiency [85]. As shown in Fig. 10(b), the pH of the adsorption medium plays a crucial role in influencing the adsorption rate. To investigate this effect, a 100 mL dye solution containing 20 mg of adsorbent at a 5 ppm concentration was prepared, and the impact of different pH levels (3, 5, 7, 9, and 11) on dye adsorption was studied. The experiment was carried out at room temperature with continuous agitation to ensure uniform mixing and adsorption efficiency. As illustrated in Fig. 11(b), the percentage of dye removal remains stable at lower pH values but decreases as the pH increases from 9 to 11, indicating reduced dye removal efficiency in more alkaline environments. This pH dependence is likely due to decreased adsorbent polarization under acidic conditions, thereby enhancing adsorption performance [86]. The photocatalytic process begins when photons (hν) with energy greater than or equal to the bandgap energy (Eg) of the photocatalyst strike its surface, exciting electrons (e^-) to the conduction band and generating holes (h^+) in the valence band, thereby initiating the degradation mechanism.

In the photocatalytic process, 3 mM concentrations of AO, IPA, or BQ were used as scavengers to target h^+•OH, and O_2^- species, respectively. The results indicate that h^+ and O_2^- species are the primary contributors to dye degradation. Since IPA had no significant effect on dye removal, it is evident that •OH radicals play a secondary role, as shown in Fig. 10(c). Furthermore, the photodegradation process is strongly influenced by the valence and conduction band potentials, which are determined by the energy gap [87]. The conduction and valence band potentials of Ag, calculated empirically from the energy gap values in Fig. 3(b), are presented in Eq. (4-5),

$$E_{CB} = X - E^{C} - 0.5E_g \dots . (4)$$

$$E_{VB} = E_{CB} + E_g \dots \dots \dots \dots (5)$$

Here, *X* represents the electronegativity of Ag (X = 4.439 eV), E^c is the energy of free electrons on the NHE scale (4.5 eV), and E and E correspond to the valence- and conduction-band potentials, respectively. Given that the band gap energy of Ag is E_g = 2.31 eV, the valence and conduction band potentials of Ag are calculated to be 1.0994 and -1.216 eV.

When aqueous dye solutions containing Ag photocatalysts are exposed to UV light, electron-hole pairs are generated, as described by Eq. (6). The excitation process allows electrons to transition from the valence band (VB) to the conduction band (CB), leaving behind holes in the VB. Upon photo-excitation, a portion of these electrons migrates to the CB, while others become trapped in localized defect states below the Ag band. This charge separation plays a crucial role in facilitating the photocatalytic degradation process. The electrons in the conduction band (CB) are rapidly transferred to the Ag nanoparticles, where they interact with the oxygen present in the dye solution to generate superoxide radicals ($O_2^{\bullet-}$), as described by Eq. (7). Additionally, the oxygen vacancies in Ag nanoparticles facilitate the movement of trapped electrons to the surface, where they accumulate. These surface-accumulated electrons react with dissolved oxygen in solution, forming $O_2^{\bullet-}$ radicals that play a crucial role in the degradation of dye molecules. At this stage, Ag acts as an electron acceptor, effectively reducing the recombination rate of photogenerated electron-hole pairs in Ag. As illustrated in Eqs. (8) and (9), the holes in Ag's valence band (VB) interact with water molecules, generating hydroxide ions (OH^-), which subsequently form hydroxyl radicals ($OH^\bullet$). These hydroxyl radicals are highly reactive and play a crucial role in the breakdown of dye molecules. Additionally, dye photosensitization is a vital factor in the photodegradation process. When the adsorbed dye molecules are exposed to light, they undergo photosensitization, thereby exciting electrons [88]. These excited electrons transition to a higher energy state and can be injected into the conduction band of Ag nanoparticles, further enhancing the photocatalytic degradation efficiency [97]. As Ag nanoparticles receive electrons, the generation of reactive species, such as superoxide radicals ($O_2^{\bullet-}$), is enhanced, thereby significantly accelerating the breakdown of dye molecules. Additionally, when $O_2^{\bullet-}$ radicals interact with protons (H^+), hydrogen peroxide (H_2O_2) is formed at the surface. These H_2O_2 molecules further react with electrons, producing additional hydroxyl radicals ($OH^\bullet$), which play a crucial role in dye degradation [89]. The Coulomb interactions between $O_2^{\bullet-}$ and $OH^\bullet$ radicals enable them to target the functional groups of RB dye molecules efficiently adsorbed onto the photocatalyst surface. This interaction results in the breakdown of complex dye structures into smaller, environmentally benign byproducts, such as CO_2, SO_4^{2-}, NO_3^-, and H_2O, as represented in Eq. (10-11) [90, 98-100],

$$\mathrm{Ag + hv \rightarrow Ag\,(h^+) + Ag\,(e^-)} \qquad (6)$$

$$\mathrm{Ag\,(e^-_{CB}) + Ag \rightarrow Ag\,(e^-) + Ag} \qquad (7)$$

$$\mathrm{Ag\,(e^-) + O_2 \rightarrow Ag + O_2^-} \qquad (8)$$

$$\mathrm{Ag\,(h^+_{VB}) + OH^- \rightarrow Ag + OH} \qquad (9)$$

$$\mathrm{O_2^{\cdot-} + 2H_2O + e^- \rightarrow 3OH^- + OH^{\cdot}} \qquad (10)$$

$$\mathrm{O_2^{\cdot-} + OH^{\cdot} + Dye \rightarrow CO_2 + H_2O} \qquad (11)$$

Table 1. Comparative study of the previously reported literature on the catalytic degradation.

Nanoparticle	Dye	Time	% D	Referecne
Ag	MB	72 h	95	[91]
Ag	MB	6 min	82	[92]
Ag	MB	150 min	97.57	[93]
Ag	MO	3 h	100	[94]
Ag	MB	1 h	99.6	[95]
Ag	MB	180 min	82.8	[96]
Ag	**MG**	**90**	**95.15**	**Present work**
	OG	**70**	**97.02**	
	RB	**110**	**94.41**	
	MV	**190**	**96.87**	

CONCLUSION

This study successfully demonstrated the green synthesis of silver nanoparticles (Ag NPs) from neem leaves via the solution combustion method, offering an eco-friendly and cost-effective approach to nanomaterial fabrication. The structural, morphological, and optical characterizations confirmed the formation of highly crystalline, uniformly distributed Ag NPs with a band gap of 2.31 eV. The synthesized nanoparticles exhibited remarkable antioxidant activity, achieving over 90% inhibition across multiple assays, indicating their potential for biomedical and pharmaceutical applications. Additionally, their exceptional photocatalytic performance against a range of azo dyes, achieving over 94% degradation efficiency within 10 minutes, underscores their viability for environmental remediation. The kinetic studies, recyclability, and scavenger analysis further validated their stability and efficacy. These findings establish Ag NPs as a promising multifunctional nanomaterial for sustainable environmental and healthcare applications, paving the way for future research in scalable production and real-world deployment.

ACKNOWLEDGEMENTS

Department of Organic Chemistry, V. V. Puram College of Science, Bangalore, Karnataka.

Funding

This research received no specific grant from any funding agency in the public, commercial,
or not-for-profit sectors

Authors' Contributions

Chethan K S: Experimental, Data Collection, and Writing.

REFERENCES

[1] B. Khodashenas, H.R. Ghorbani, Synthesis of silver nanoparticles with different shapes, Arabian Journal of Chemistry 12 (2019) 1823–1838. https://doi.org/10.1016/j.arabjc.2014.12.014.

[2] W.N.A. Wan Osman, M.H. Rosli, W.N.A. Mazli, S. Samsuri, Comparative review of biodiesel production and purification, Carbon Capture Science & Technology 13 (2024) 100264. https://doi.org/10.1016/j.ccst.2024.100264.

[3] S. Kumari, S. Raturi, S. Kulshrestha, K. Chauhan, S. Dhingra, K. András, K. Thu, R. Khargotra, T. Singh, A comprehensive review on various techniques used for synthesizing nanoparticles, Journal of Materials Research and Technology 27 (2023) 1739–1763. https://doi.org/10.1016/j.jmrt.2023.09.291.

[4] L. Xu, D. Liu, D. Chen, H. Liu, J. Yang, Size and shape controlled synthesis of rhodium nanoparticles, Heliyon 5 (2019) e01165. https://doi.org/10.1016/j.heliyon.2019.e01165.

[5] S.F. Ahmed, M. Mofijur, N. Rafa, A.T. Chowdhury, S. Chowdhury, M. Nahrin, A.B.M.S. Islam, H.C. Ong, Green approaches in synthesising nanomaterials for environmental nanobioremediation: Technological advancements, applications, benefits and challenges, Environmental Research 204 (2022) 111967. https://doi.org/10.1016/j.envres.2021.111967.

[6] C. Krishnaraj, E.G. Jagan, S. Rajasekar, P. Selvakumar, P.T. Kalaichelvan, N. Mohan, Synthesis of silver nanoparticles using Acalypha indica leaf extracts and its antibacterial activity against water borne pathogens, Colloids and Surfaces B: Biointerfaces 76 (2010) 50–56. https://doi.org/10.1016/j.colsurfb.2009.10.008.

[7] Y. Zhou, S.H. Yu, X.P. Cui, C.Y. Wang, Z.Y. Chen, Formation of Silver Nanowires by a Novel Solid−Liquid Phase Arc Discharge Method, Chem. Mater. 11 (1999) 545–546. https://doi.org/10.1021/cm981122h.

[8] M.I. Husseiny, M.A. El-Aziz, Y. Badr, M.A. Mahmoud, Biosynthesis of gold nanoparticles using Pseudomonas aeruginosa, Spectrochimica Acta Part A: Molecular and Biomolecular Spectroscopy 67 (2007) 1003–1006. https://doi.org/10.1016/j.saa.2006.09.028.

[9] U. Kumar Sur, B. Ankamwar, S. Karmakar, A. Halder, P. Das, Green synthesis of Silver nanoparticles using the plant extract of Shikakai and Reetha, Materials Today: Proceedings 5 (2018) 2321–2329. https://doi.org/10.1016/j.matpr.2017.09.236.

[10] N.C. Sharma, S.V. Sahi, S. Nath, J.G. Parsons, J.L. Gardea- Torresde, T. Pal, Synthesis of Plant-Mediated Gold Nanoparticles and Catalytic Role of Biomatrix-Embedded Nanomaterials, Environ. Sci. Technol. 41 (2007) 5137–5142. https://doi.org/10.1021/es062929a.

[11] S. Rathod, S. Preetam, C. Pandey, S.P. Bera, Exploring synthesis and applications of green nanoparticles and the role of nanotechnology in wastewater treatment, Biotechnology Reports 41 (2024) e00830. https://doi.org/10.1016/j.btre.2024.e00830.

[12] S. Ying, Z. Guan, P.C. Ofoegbu, P. Clubb, C. Rico, F. He, J. Hong, Green synthesis of nanoparticles: Current developments and limitations, Environmental Technology & Innovation 26 (2022) 102336. https://doi.org/10.1016/j.eti.2022.102336.

[13] T. Bruna, F. Maldonado-Bravo, P. Jara, N. Caro, Silver Nanoparticles and Their Antibacterial Applications, IJMS 22 (2021) 7202. https://doi.org/10.3390/ijms22137202.

[14] V. Ravichandran, S. Vasanthi, S. Shalini, S.A.A. Shah, M. Tripathy, N. Paliwal, Green synthesis, characterization, antibacterial, antioxidant and photocatalytic activity of Parkia speciosa leaves extract mediated silver nanoparticles, Results in Physics 15 (2019) 102565. https://doi.org/10.1016/j.rinp.2019.102565.

[15] I. Fatimah, Green synthesis of silver nanoparticles using extract of Parkia speciosa Hassk pods assisted by microwave irradiation, Journal of Advanced Research 7 (2016) 961–969. https://doi.org/10.1016/j.jare.2016.10.002.

[16] K.N. Yusof, S.S. Alias, Z. Harun, H. Basri, F.H. Azhar, *Parkia speciosa* as Reduction Agent in Green Synthesis Silver Nanoparticles, ChemistrySelect 3 (2018) 8881–8885. https://doi.org/10.1002/slct.201801846.

[17] H.S. El-Beltagi, M. Ragab, A. Osman, R.A. El-Masry, K.M. Alwutayd, H. Althagafi, L.S. Alqahtani, R.S. Alazragi, A.S. Alhajri, M.M. El-Saber, Biosynthesis of zinc oxide nanoparticles *via* neem extract and their anticancer and antibacterial activities, PeerJ 12 (2024) e17588. https://doi.org/10.7717/peerj.17588.

[18] A. Dhaka, S. Chand Mali, S. Sharma, R. Trivedi, A review on biological synthesis of silver nanoparticles and their potential applications, Results in Chemistry 6 (2023) 101108. https://doi.org/10.1016/j.rechem.2023.101108.

[19] S.A. Kumari, A.K. Patlolla, P. Madhusudhanachary, Biosynthesis of Silver Nanoparticles Using Azadirachta indica and Their Antioxidant and Anticancer Effects in Cell Lines, Micromachines 13 (2022) 1416. https://doi.org/10.3390/mi13091416.

[20] A. Zanjage, S.A. Khan, Ultra-fast synthesis of antibacterial and photo catalyst silver nanoparticles using neem leaves, JCIS Open 3 (2021) 100015. https://doi.org/10.1016/j.jciso.2021.100015.

[21] A. Shankar, V. Kumar, N.K. Kaushik, A. Kumar, V. Malik, D. Singh, B. Singh, Sporotrichum thermophile culture extract-mediated greener synthesis of silver nanoparticles: Eco-friendly functional group transformation and anti-bacterial study, Current Research in Green and Sustainable Chemistry 3 (2020) 100029. https://doi.org/10.1016/j.crgsc.2020.100029.

[22] D. Garg, A. Sarkar, P. Chand, P. Bansal, D. Gola, S. Sharma, S. Khantwal, Surabhi, R. Mehrotra, N. Chauhan, R.K. Bharti, Synthesis of silver nanoparticles utilizing various biological systems: mechanisms and applications-a review, Prog Biomater 9 (2020) 81–95. https://doi.org/10.1007/s40204-020-00135-2.

[23] K. Karthik, M. Shashank, V. Revathi, T. Tatarchuk, Facile microwave-assisted green synthesis of NiO nanoparticles from *Andrographis paniculata* leaf extract and evaluation of their photocatalytic and anticancer activities, Molecular Crystals and Liquid Crystals 673 (2018) 70–80. https://doi.org/10.1080/15421406.2019.1578495.

[24] K. Gudikandula, S. Charya Maringanti, Synthesis of silver nanoparticles by chemical and biological methods and their antimicrobial properties, Journal of Experimental Nanoscience 11 (2016) 714–721. https://doi.org/10.1080/17458080.2016.1139196.

[25] P. Mathur, S. Saini, E. Paul, C. Sharma, P. Mehtani, Endophytic fungi mediated synthesis of iron nanoparticles: Characterization and application in methylene blue decolorization, Current Research in Green and Sustainable Chemistry 4 (2021) 100053. https://doi.org/10.1016/j.crgsc.2020.100053.

[26] S.S. Royji Albeladi, M.A. Malik, S.A. Al-thabaiti, Facile biofabrication of silver nanoparticles using Salvia officinalis leaf extract and its catalytic activity towards Congo red dye degradation, Journal of Materials Research and Technology 9 (2020) 10031–10044. https://doi.org/10.1016/j.jmrt.2020.06.074.

[27] P.C.L. Muraro, S.R. Mortari, B.S. Vizzotto, G. Chuy, C. Dos Santos, L.F.W. Brum, W.L. Da Silva, Iron oxide nanocatalyst with titanium and silver nanoparticles: Synthesis, characterization and photocatalytic activity on the degradation of Rhodamine B dye, Sci Rep 10 (2020) 3055. https://doi.org/10.1038/s41598-020-59987-0.

[28] M. Chandhru, S. Kutti Rani, N. Vasimalai, Reductive degradation of toxic six dyes in industrial wastewater using diaminobenzoic acid capped silver nanoparticles, Journal of Environmental Chemical Engineering 8 (2020) 104225. https://doi.org/10.1016/j.jece.2020.104225.

[29] S. Pandey, J.Y. Do, J. Kim, M. Kang, Fast and highly efficient catalytic degradation of dyes using κ-carrageenan stabilized silver nanoparticles nanocatalyst, Carbohydrate Polymers 230 (2020) 115597. https://doi.org/10.1016/j.carbpol.2019.115597.

[30] K. Chand, D. Cao, D. Eldin Fouad, A. Hussain Shah, A. Qadeer Dayo, K. Zhu, M. Nazim Lakhan, G. Mehdi, S. Dong, Green synthesis, characterization and photocatalytic application of silver nanoparticles synthesized by various plant extracts, Arabian Journal of Chemistry 13 (2020) 8248–8261. https://doi.org/10.1016/j.arabjc.2020.01.009.

[31] A. Nazir, S. Farooq, M. Abbas, E.A. Alabbad, H. Albalawi, N. Alwadai, A.H. Almuqrin, M. Iqbal, Synthesis, characterization and photocatalytic application of *Sophora mollis* leaf extract mediated silver nanoparticles, Zeitschrift Für Physikalische Chemie 235 (2021) 1589–1607. https://doi.org/10.1515/zpch-2020-1803.

[32] M. Rafique, I. Sadaf, M.B. Tahir, M.S. Rafique, G. Nabi, T. Iqbal, K. Sughra, Novel and facile synthesis of silver nanoparticles using Albizia procera leaf extract for dye degradation and antibacterial applications, Materials Science and Engineering: C 99 (2019) 1313–1324. https://doi.org/10.1016/j.msec.2019.02.059.

[33] A. Jain, F. Ahmad, D. Gola, A. Malik, N. Chauhan, P. Dey, P.K. Tyagi, Multi dye degradation and antibacterial potential of Papaya leaf derived silver nanoparticles, Environmental Nanotechnology, Monitoring & Management 14 (2020) 100337. https://doi.org/10.1016/j.enmm.2020.100337.

[34] D. Gola, A. Kriti, N. Bhatt, M. Bajpai, A. Singh, A. Arya, N. Chauhan, S.K. Srivastava, P.K. Tyagi, Y. Agrawal, Silver nanoparticles for enhanced dye degradation, Current Research in Green and Sustainable Chemistry 4 (2021) 100132. https://doi.org/10.1016/j.crgsc.2021.100132.

[35] M. Mathur, D. Gola, R. Panja, A. Malik, S.Z. Ahammad, Performance evaluation of two Aspergillus spp. for the decolourization of reactive dyes by bioaccumulation and biosorption, Environ Sci Pollut Res 25 (2018) 345–352. https://doi.org/10.1007/s11356-017-0417-0.

[36] M.C. Roopa, S. Thirumala, S. Kallimani, B.M. Manohara, Green synthesis and characterization of nano reduced graphene oxide/cerium oxide (rGO/CeO_2) for Rose Bengal dye degradation, Journal of Alloys and Compounds Communications 4 (2024) 100033. https://doi.org/10.1016/j.jacomc.2024.100033.

[37] F. Lalsangpuii, S.L. Rokhum, F. Nghakliana, L. Fakawmi, J.V.L. Ruatpuia, E. Laltlanmawii, R. Lalfakzuala, Z. Siama, Green Synthesis of Silver Nanoparticles Using *Spilanthes acmella* Leaf Extract and its Antioxidant-Mediated Ameliorative Activity against Doxorubicin-Induced Toxicity in Dalton's Lymphoma Ascites (DLA)-Bearing Mice, ACS Omega 7 (2022) 44346–44359. https://doi.org/10.1021/acsomega.2c05970.

[38] B.K. Mehta, M. Chhajlani, B.D. Shrivastava, Green synthesis of silver nanoparticles and their characterization by XRD, J. Phys.: Conf. Ser. 836 (2017) 012050. https://doi.org/10.1088/1742-6596/836/1/012050.

[39] M.C. Roopa, S. Thirumala, S. Kallimani, B.M. Manohara, Green and Reflux method synthesis of CeO_2/rGO for their characterization and Photodegradation of dye, Sustainable Chemistry One World 4 (2024) 100024. https://doi.org/10.1016/j.scowo.2024.100024.

[40] V.S. Vinila, J. Isac, Synthesis and structural studies of superconducting perovskite $GdBa_2Ca_3Cu_4O_{10.5+\delta}$ nanosystems, in: Design, Fabrication, and Characterization of Multifunctional Nanomaterials, Elsevier, 2022: pp. 319–341. https://doi.org/10.1016/B978-0-12-820558-7.00022-4.

[41] L. Karthik, G. Kumar, A.V. Kirthi, A.A. Rahuman, K.V. Bhaskara Rao, Streptomyces sp. LK3 mediated synthesis of silver nanoparticles and its biomedical application, Bioprocess Biosyst Eng 37 (2014) 261–267. https://doi.org/10.1007/s00449-013-0994-3.

[42] K. Jyoti, M. Baunthiyal, A. Singh, Characterization of silver nanoparticles synthesized using Urtica dioica Linn. leaves and their synergistic effects with antibiotics, Journal of Radiation Research and Applied Sciences 9 (2016) 217–227. https://doi.org/10.1016/j.jrras.2015.10.002.

[43] F. Zia, N. Ghafoor, M. Iqbal, S. Mehboob, Green synthesis and characterization of silver nanoparticles using Cydonia oblong seed extract, Appl Nanosci 6 (2016) 1023–1029. https://doi.org/10.1007/s13204-016-0517-z.

[44] W.K.A. Wan Mat Khalir, K. Shameli, S.D. Jazayeri, N.A. Othman, N.W. Che Jusoh, N.M. Hassan, Biosynthesized Silver Nanoparticles by Aqueous Stem Extract of Entada spiralis and Screening of Their Biomedical Activity, Front. Chem. 8 (2020) 620. https://doi.org/10.3389/fchem.2020.00620.

[45] K. C., S. S., S.M. G., K. S., A FTIR approach of green synthesized silver nanoparticles by *Ocimum sanctum* and *Ocimum gratissimum* on mung bean seeds, Inorganic and Nano-Metal Chemistry 50 (2020) 606–612. https://doi.org/10.1080/24701556.2020.1723025.

[46] K. Ramar, G. Gnanamoorthy, D. Mukundan, R. Vasanthakumari, V. Narayanan, A. Jafar Ahamed, Environmental and antimicrobial properties of silver nanoparticles synthesized using Azadirachta indica Juss leaves extract, SN Appl. Sci. 1 (2019) 128. https://doi.org/10.1007/s42452-018-0143-3.

[47] M.Y. Berezin, S. Achilefu, Fluorescence Lifetime Measurements and Biological Imaging, Chem. Rev. 110 (2010) 2641–2684. https://doi.org/10.1021/cr900343z.

[48] H.T. Fan, S.S. Pan, X.M. Teng, C. Ye, G.H. Li, L.D. Zhang, δ-Bi_2O_3 thin films prepared by reactive sputtering: Fabrication and characterization, Thin Solid Films 513 (2006) 142–147. https://doi.org/10.1016/j.tsf.2006.01.074.

[49] H. Patel, J. Joshi, Green and chemical approach for synthesis of Ag_2O nanoparticles and their antimicrobial activity, J Sol-Gel Sci Technol (2023). https://doi.org/10.1007/s10971-023-06036-7.

[50] I.A.M. Ali, A.B. Ahmed, H.I. Al-Ahmed, Green synthesis and characterization of silver nanoparticles for reducing the damage to sperm parameters in diabetic compared to metformin, Sci Rep 13 (2023) 2256. https://doi.org/10.1038/s41598-023-29412-3.

[51] H. Tiwari, K. Samal, S.R. Geed, S. Bera, C. Das, K. Mohanty, Green synthesis of silver nanoparticles for ultrafiltration membrane surface modification and antimicrobial activity, Sustainable Chemistry for Climate Action 3 (2023) 100031. https://doi.org/10.1016/j.scca.2023.100031.

[52] P. Bhuyar, M.H.Ab. Rahim, S. Sundararaju, R. Ramaraj, G.P. Maniam, N. Govindan, Synthesis of silver nanoparticles using marine macroalgae Padina sp. and its antibacterial activity towards pathogenic bacteria, Beni-Suef Univ J Basic Appl Sci 9 (2020) 3. https://doi.org/10.1186/s43088-019-0031-y.

[53] N. Chandimali, S.G. Bak, E.H. Park, H.-J. Lim, Y.-S. Won, E.-K. Kim, S.-I. Park, S.J. Lee, Free radicals and their impact on health and antioxidant defenses: a review, Cell Death Discov. 11 (2025) 19. https://doi.org/10.1038/s41420-024-02278-8.

[54] A. Floegel, D.-O. Kim, S.-J. Chung, S.I. Koo, O.K. Chun, Comparison of ABTS/DPPH assays to measure antioxidant capacity in popular antioxidant-rich US foods, Journal of Food Composition and Analysis 24 (2011) 1043–1048. https://doi.org/10.1016/j.jfca.2011.01.008.

[55] N. Bibi Sadeer, D. Montesano, S. Albrizio, G. Zengin, M.F. Mahomoodally, The Versatility of Antioxidant Assays in Food Science and Safety—Chemistry, Applications, Strengths, and Limitations, Antioxidants 9 (2020) 709. https://doi.org/10.3390/antiox9080709.

[56] S. Baliyan, R. Mukherjee, A. Priyadarshini, A. Vibhuti, A. Gupta, R.P. Pandey, C.-M. Chang, Determination of Antioxidants by DPPH Radical Scavenging Activity and Quantitative Phytochemical Analysis of Ficus religiosa, Molecules 27 (2022) 1326. https://doi.org/10.3390/molecules27041326.

[57] R. Apak, M. Özyürek, K. Güçlü, E. Çapanoğlu, Antioxidant Activity/Capacity Measurement. 1. Classification, Physicochemical Principles, Mechanisms, and Electron Transfer (ET)-Based Assays, J. Agric. Food Chem. 64 (2016) 997–1027. https://doi.org/10.1021/acs.jafc.5b04739.

[58] I.G. Munteanu, C. Apetrei, Analytical Methods Used in Determining Antioxidant Activity: A Review, IJMS 22 (2021) 3380. https://doi.org/10.3390/ijms22073380.

[59] Md.M. Rahman, Md.B. Islam, M. Biswas, A.H.M. Khurshid Alam, In vitro antioxidant and free radical scavenging activity of different parts of Tabebuia pallida growing in Bangladesh, BMC Res Notes 8 (2015) 621. https://doi.org/10.1186/s13104-015-1618-6.

[60] İ. Gulcin, S.H. Alwasel, DPPH Radical Scavenging Assay, Processes 11 (2023) 2248. https://doi.org/10.3390/pr11082248.

[61] M. Spiegel, K. Kapusta, W. Kołodziejczyk, J. Saloni, B. Żbikowska, G.A. Hill, Z. Sroka, Antioxidant Activity of Selected Phenolic Acids–Ferric Reducing Antioxidant Power Assay and QSAR Analysis of the Structural Features, Molecules 25 (2020) 3088. https://doi.org/10.3390/molecules25133088.

[62] M.C. Christodoulou, J.C. Orellana Palacios, G. Hesami, S. Jafarzadeh, J.M. Lorenzo, R. Domínguez, A. Moreno, M. Hadidi, Spectrophotometric Methods for Measurement of Antioxidant Activity in Food and Pharmaceuticals, Antioxidants 11 (2022) 2213. https://doi.org/10.3390/antiox11112213.

[63] G. Marc, A. Stana, S.D. Oniga, A. Pîrnău, L. Vlase, O. Oniga, New Phenolic Derivatives of Thiazolidine-2,4-dione with Antioxidant and Antiradical Properties: Synthesis, Characterization, In Vitro Evaluation, and Quantum Studies, Molecules 24 (2019) 2060. https://doi.org/10.3390/molecules24112060.

[64] I.G. Munteanu, C. Apetrei, Analytical Methods Used in Determining Antioxidant Activity: A Review, IJMS 22 (2021) 3380. https://doi.org/10.3390/ijms22073380.

[65] I.F.F. Benzie, M. Devaki, The ferric reducing/antioxidant power (FRAP) assay for non-enzymatic antioxidant capacity: concepts, procedures, limitations and applications, in: R. Apak, E. Capanoglu, F. Shahidi (Eds.), Measurement of Antioxidant Activity & Capacity, John Wiley & Sons, Ltd, Chichester, UK, 2017: pp. 77–106. https://doi.org/10.1002/9781119135388.ch5.

[66] G. Liu, P. Men, G. Perry, M.A. Smith, Nanoparticle and Iron Chelators as a Potential Novel Alzheimer Therapy, in: R.M. Uppu, S.N. Murthy, W.A. Pryor, N.L. Parinandi (Eds.), Free Radicals and Antioxidant Protocols, Humana Press, Totowa, NJ, 2010: pp. 123–144. https://doi.org/10.1007/978-1-60327-029-8_8.

[67] I. Farahanah, S. Sahudin, H.F. Mohsin, S.A. Ariffin, L.D. Aminuddin, Understanding Investigational Perspective of Antioxidant and Antibacterial Properties of Rice, Rice Science 32 (2025) 15–31. https://doi.org/10.1016/j.rsci.2024.10.004.

[68] R. Sudan, M. Bhagat, S. Gupta, J. Singh, A. Koul, Iron (FeII) Chelation, Ferric Reducing Antioxidant Power, and Immune Modulating Potential of *Arisaema jacquemontii* (Himalayan Cobra Lily), BioMed Research International 2014 (2014) 1–7. https://doi.org/10.1155/2014/179865.

[69] S.A. Mousa, D.A. Wissa, H.H. Hassan, A.A. Ebnalwaled, S.A. Khairy, Enhanced photocatalytic activity of green synthesized zinc oxide nanoparticles using low-cost plant extracts, Sci Rep 14 (2024) 16713. https://doi.org/10.1038/s41598-024-66975-1.

[70] S. K K, P.N. P M, M. Vasundhara, Enhanced photocatalytic activity in ZnO nanoparticles developed using novel *Lepidagathis ananthapuramensis* leaf extract, RSC Adv. 13 (2023) 1497–1515. https://doi.org/10.1039/D2RA06967A.

[71] A. Chauhan, R. Verma, S. Kumari, A. Sharma, P. Shandilya, X. Li, K.M. Batoo, A. Imran, S. Kulshrestha, R. Kumar, Photocatalytic dye degradation and antimicrobial activities of Pure and Ag-doped ZnO using Cannabis sativa leaf extract, Sci Rep 10 (2020) 7881. https://doi.org/10.1038/s41598-020-64419-0.

[72] N.T. Nguyen, V.A. Nguyen, Synthesis, Characterization, and Photocatalytic Activity of ZnO Nanomaterials Prepared by a Green, Nonchemical Route, Journal of Nanomaterials 2020 (2020) 1–8. https://doi.org/10.1155/2020/1768371.

[73] S.S. Wagh, V.S. Kadam, C.V. Jagtap, D.B. Salunkhe, R.S. Patil, H.M. Pathan, S.P. Patole, Comparative Studies on Synthesis, Characterization and Photocatalytic Activity of Ag Doped ZnO Nanoparticles, ACS Omega 8 (2023) 7779–7790. https://doi.org/10.1021/acsomega.2c07499.

[74] . Shkir, B.M. Al-Shehri, M.P. Pachamuthu, A. Khan, K.V. Chandekar, S. AlFaify, M.S. Hamdy, A remarkable improvement in photocatalytic activity of ZnO nanoparticles through Sr doping synthesized by one pot flash combustion technique for water treatments, Colloids and Surfaces A: Physicochemical and Engineering Aspects 587 (2020) 124340. https://doi.org/10.1016/j.colsurfa.2019.124340.

[75] Y. Hendrix, E. Rauwel, K. Nagpal, R. Haddad, E. Estephan, C. Boissière, P. Rauwel, Revealing the Dependency of Dye Adsorption and Photocatalytic Activity of ZnO Nanoparticles on Their Morphology and Defect States, Nanomaterials 13 (2023) 1998. https://doi.org/10.3390/nano13131998.

[76] L.M. Jose, R.S.A. Raj, D. Sajan, A. Aravind, Adsorption and photocatalytic activity of biosynthesised ZnO nanoparticles using Aloe Vera leaf extract, Nano Ex. 2 (2021) 010039. https://doi.org/10.1088/2632-959X/abeec6.

[77] M.S. Azmina, R. Md Nor, H.A. Rafaie, N.S.A. Razak, S.F.A. Sani, Z. Osman, Enhanced photocatalytic activity of ZnO nanoparticles grown on porous silica microparticles, Appl Nanosci 7 (2017) 885–892. https://doi.org/10.1007/s13204-017-0626-3.

[78] S. Abou Zeid, Y. Leprince-Wang, Advancements in ZnO-Based Photocatalysts for Water Treatment: A Comprehensive Review, Crystals 14 (2024) 611. https://doi.org/10.3390/cryst14070611.

[79] A. Ahmad, M.S. Javed, S. Khan, T.M. Almutairi, A.A.A. Mohammed, R. Luque, Green synthesized Ag decorated CeO_2 nanoparticles: Efficient photocatalysts and potential antibacterial agents., Chemosphere 310 (2023) 136841. https://doi.org/10.1016/j.chemosphere.2022.136841.

[80] G. Ramanathan, S.V. Rathan, K.R. Murali, Photocatalytic activity of biosynthesized CeO2 nano particles, SN Appl. Sci. 1 (2019) 116. https://doi.org/10.1007/s42452-018-0103-y.

[81] D. Toloman, A. Popa, R.B. Sonher, R. Bortnic, T.F. Marinca, I. Perhaita, M. Filip, A. Mesaros, Enhancing the Photocatalytic Activity and Luminescent Properties of Rare-Earth-Doped CeO_2 Nanoparticles, Applied Sciences 14 (2024) 522. https://doi.org/10.3390/app14020522.

[82] S. Zhao, M. Riedel, J. Patarroyo, N.G. Bastús, V. Puntes, Z. Yue, F. Lisdat, W.J. Parak, Tailoring of the photocatalytic activity of CeO_2 nanoparticles by the presence of plasmonic Ag nanoparticles, Nanoscale 14 (2022) 12048–12059. https://doi.org/10.1039/D2NR01318E.

[83] G. Murugadoss, D.D. Kumar, M.R. Kumar, N. Venkatesh, P. Sakthivel, Silver decorated CeO_2 nanoparticles for rapid photocatalytic degradation of textile rose bengal dye, Sci Rep 11 (2021) 1080. https://doi.org/10.1038/s41598-020-79993-6.

[84] A.A. Atran, F.A. Ibrahim, N.S. Awwad, H.S.M. Abd-Rabboh, M.S. Hamdy, Remarkable enhancement in the photocatalytic activity of porous CeO2 nanoparticles through nickel doping for wastewater treatment, J Mater Sci: Mater Electron 34 (2023) 2082. https://doi.org/10.1007/s10854-023-11554-9.

[85] A.S. Belousov, E.V. Suleimanov, A.A. Parkhacheva, D.G. Fukina, A.V. Koryagin, A.V. Koroleva, E.V. Zhizhin, A.P. Gorshkov, Regulating of MnO_2 photocatalytic activity in degradation of organic dyes by polymorphic engineering, Solid State Sciences 132 (2022) 106997. https://doi.org/10.1016/j.solidstatesciences.2022.106997.

[86] V. Arumugaperumal, S. K, Solar light driven photocatalytic degradation of methylene blue dye over Cu doped α-MnO_2 nanoparticles, Chemical Physics Impact 8 (2024) 100434. https://doi.org/10.1016/j.chphi.2023.100434.

[87] H.L. Haile, T. Abi, K. Tesfahun, Synthesis, characterization and photocatalytic activity of $MnO_2/Al_2O_3/Fe_2O_3$ nanocomposite for degradation of malachite green, Afr. J. Pure Appl. Chem. 9 (2015) 211–222. https://doi.org/10.5897/AJPAC2015.0656.

[88] M.F. Warsi, M. Bilal, S. Zulfiqar, M.U. Khalid, P.O. Agboola, I. Shakir, Enhanced visible light driven Photocatalytic activity of MnO_2 nanomaterials and their hybrid structure with carbon nanotubes, Mater. Res. Express 7 (2020) 105015. https://doi.org/10.1088/2053-1591/abbf8d.

[89] M.Z.A. Warshagha, M. Muneer, Direct Z-Scheme AgBr/β-MnO_2 Photocatalysts for Highly Efficient Photocatalytic and Anticancer Activity, ACS Omega 7 (2022) 30171–30183. https://doi.org/10.1021/acsomega.2c03260.

[90] K. Fan, Q. Chen, J. Zhao, Y. Liu, Preparation of MnO_2-Carbon Materials and Their Applications in Photocatalytic Water Treatment, Nanomaterials 13 (2023) 541. https://doi.org/10.3390/nano13030541.

[91] M. Vanaja, K. Paulkumar, M. Baburaja, S. Rajeshkumar, G. Gnanajobitha, C. Malarkodi, M. Sivakavinesan, G. Annadurai, Degradation of Methylene Blue Using Biologically Synthesized Silver Nanoparticles, Bioinorganic Chemistry and Applications 2014 (2014) 1–8. https://doi.org/10.1155/2014/742346.

[92] S.A. Ogundare, T.O. Adesetan, G. Muungani, V. Moodley, J.F. Amaku, O.C. Atewolara-Odule, S.T. Yussuf, N.O. Sanyaolu, A.A. Ibikunle, M.-S. Balogun, W. Ewald Van Zyl, Catalytic degradation of methylene blue dye and antibacterial activity of biosynthesized silver nanoparticles using *Peltophorum pterocarpum* (DC.) leaves, Environ. Sci.: Adv. 2 (2023) 247–256. https://doi.org/10.1039/D2VA00164K.

[93] J. Kadam, P. Dhawal, S. Barve, S. Kakodkar, Green synthesis of silver nanoparticles using cauliflower waste and their multifaceted applications in photocatalytic degradation of methylene blue dye and Hg^{2+} biosensing, SN Appl. Sci. 2 (2020) 738. https://doi.org/10.1007/s42452-020-2543-4.

[94] B.S. Muthukrishnan S, S.M. Muthukumar M, S.K.T. Rao Mv, Catalytic Degradation of Organic Dyes using Synthesized Silver Nanoparticles: A Green Approach, J Bioremed Biodeg 06 (2015). https://doi.org/10.4172/2155-6199.1000312.

[95] M. Rafique, I. Sadaf, M.B. Tahir, M.S. Rafique, G. Nabi, T. Iqbal, K. Sughra, Novel and facile synthesis of silver nanoparticles using Albizia procera leaf extract for dye degradation and antibacterial applications, Materials Science and Engineering: C 99 (2019) 1313–1324. https://doi.org/10.1016/j.msec.2019.02.059.

[96] J. Singh, A.S. Dhaliwal, Plasmon-induced photocatalytic degradation of methylene blue dye using biosynthesized silver nanoparticles as photocatalyst, Environmental Technology 41 (2020) 1520–1534. https://doi.org/10.1080/09593330.2018.1540663.

[97] V. Hoseinpour, M. Souri, N. Ghaemi, Green synthesis, characterisation, and photocatalytic activity of manganese dioxide nanoparticles, Micro & Nano Letters 13 (2018) 1560–1563. https://doi.org/10.1049/mnl.2018.5008.

[98] S. Taghavi Fardood, F. Moradnia, F. Yekke Zare, S. Heidarzadeh, M. Azad Majedi, A. Ramazani, M. Sillanpää, K. Nguyen, Green synthesis and characterization of α-Mn_2O_3 nanoparticles for antibacterial activity and efficient visible-light photocatalysis, Sci Rep 14 (2024) 6755. https://doi.org/10.1038/s41598-024-56666-2.

[99] Y.-L. Chan, S.-Y. Pung, S. Sreekantan, F.-Y. Yeoh, Photocatalytic activity of β-MnO_2 nanotubes grown on PET fibre under visible light irradiation, Journal of Experimental Nanoscience 11 (2016) 603–618. https://doi.org/10.1080/17458080.2015.1102342.

[100] S. Mondal, Fabrication of MnO_2 Nanoparticles from Simple Pyrolytic Method for Degradation of Methylene Blue Under Visible Light Irradiation, Orient. J. Chem 38 (2022) 172–176. https://doi.org/10.13005/ojc/380121.